Hindawi
International Journal of Antennas and Propagation
Volume 2021, Article ID 9915688, 9 pages
https://doi.org/10.1155/2021/9915688

Research Article

The Mono/Bistatic SAR Imaging Simulation of Sea Surface with Breaking Waves Based on a Refined Facet Scattering Field Model

Ye Zhao, Wen-Tao Guan, and Peng-Ju Yang

School of Physics and Electronic Information, Yan'an University, Yan'an 716000, China

Correspondence should be addressed to Ye Zhao; zhaoye07074135@163.com

Received 8 March 2021; Revised 21 June 2021; Accepted 5 July 2021; Published 12 July 2021

Academic Editor: Giuseppe Castaldi

In order to analyze the scattering characteristics of sea surface under high sea state, a complete scattering model of sea surface considering breaking wave is established in this study based on the refined facet scattering field model (RFSFM) and the scattering theory of breaking wave. On the basis of this model, the influence of breaking waves on the mono/bistatic SAR imaging of sea surface at HH and VV polarization is studied. The results show that with the increase in wind speed, the coverage of breaking wave increases obviously and the consideration of breaking wave has a good correction for the scattering coefficient at HH polarization under grazing incidence; however, for VV polarization, the effect of breaking wave is very small.

1. Introduction

Radar plays an increasingly important role in the detection and identification of targets in marine environment. When the electromagnetic wave emitted by radar irradiates on the complex marine environment, the received scattering echo not only contains the shape, position, motion state, and other information of the target on sea surface but also inevitably contains the information of the sea surface. Therefore, the establishment of a more realistic electromagnetic model to study the electromagnetic scattering characteristics of complex marine environment is of great significance to fully understand the marine environment [1–4].

As a high resolution microwave detection device, SAR is famous for its ability to obtain target image information in complex environment. By fully understanding the complex scattering mechanism of sea surface, the SAR images can be obtained to monitor the complex marine environment. Based on this, many scholars have done decades of research on the imaging mechanism of marine SAR [5–8]. Alpers [9] analyzed SAR images of ocean waves based on the velocity bunching (VB) model. Lyzenga [10] proposed a model with time dependence. Hager [11] proposed a distributed surface (DS) model, in which the radar echoes of short-wave are regarded as uncorrelated spatially. Nunziata [12] developed a SAR sea surface wave simulator based on the velocity bunching theory. Migliaccio [13] experimentally analyzed the SAR ocean speckle intensity K-distribution model versus sea surface wind field. Rizaev [14] presented a universal simulation framework for SAR imagery of the sea surface based on the linear theory of sea surface modeling, Michell thin-ship theory for Kelvin wake modeling, and ocean SAR imaging theory. Xu [15] deeply studied the simulation of SAR echo signal in complex ocean environment by using the four-path model and high frequency calculation method. Jin et al. [16] studied the bistatic scattering and transmission of the sea surface using the forward-backward method with the spectral accelerate algorithm (FBM/SAA) method. Zhang et al. [17, 18] studied the bistatic SAR imagery of sea surface using the extended nonlinear chirp scaling algorithm and bistatic SAR image of composite ship-ocean scene based on the four-path model. Through the efforts of many scholars, the exploration, exploitation, and utilization of the complex marine environment have been greatly promoted.

In general, the sea surface will show complex features at high sea state including breaking waves. When the radar works at grazing incidence, the results of Bragg scattering mechanism are quite different from the actual measurement results, which cannot explain the phenomenon of sea spike

and high polarization ratio caused by breaking waves [19–22]. Therefore, it is of great significance to establish an electromagnetic model to study the scattering echo of sea surface with breaking waves at high sea state. In this paper, the nonlinear Creamer model is used to simulate the geometry of sea surface, and the refined facet scattering field model (RFSFM) together with the scattering theory of breaking waves is used to study the electromagnetic scattering of sea surface. Finally, the mono/bistatic SAR imaging of sea surface is simulated and discussed when the breaking waves are contained.

2. Position Distribution of Breaking Wave

In order to obtain the position distribution of breaking wave on the sea surface reasonably, in this paper, the geometric criterion proposed by Longuet-Higgins is used to judge whether the wave is a breaking wave; that is, when the slope at a certain position of the sea surface is greater than 0.586, it is regarded as a breaking wave [23]. It should be pointed out that in the simulation, the sea surface is discretized by many small facets with a certain size, and the size of facet will have an influence on the slope distribution of sea surface. Therefore, it is necessary to select an appropriate discrete interval to simulate the sea surface to ensure the correctness of the coverage rate of the breaking waves under a certain wind speed. Monahan's empirical model [24] based on the measured data is used as a reference to verify whether the coverage rate of breaking wave obtained by simulation is reasonable, and the relationship between the coverage of breaking waves and the wind speed u_{10} (m/s) at the height of 10 meters above the sea surface can be expressed as

$$W_b = 3.16 \times 10^{-7} u_{10}^{3.2}. \tag{1}$$

Figures 1(a) and 1(b) show the distribution of breaking points on sea surface when the wind speed is 10 m/s and 15 m/s. The 2D sea surface is generated using the nonlinear Creamer sea surface model, the sampling number is $M = N = 512$, and the discrete interval $\Delta x = \Delta y = 0.85$. From Figures 1(a) and 1(b), it could be obviously found that when the wind speed is 10 m/s, the distribution of breaking points on the sea surface is only a few, and when the wind speed is 15 m/s, the breaking points on the sea surface have gradually increased. And with the increase in wind speed, there will be a more obvious increase for the number of breaking points.

Figure 2 gives the comparison between the simulated coverage of the breaking waves and the measured model at different wind speeds. From Figure 2, it could be found that with the increase in wind speed, the coverage of breaking wave increases obviously, and there is an excellent agreement between the simulation results and those obtained by the Monahan formula. So far, relatively reliable and stable breaking wave coverage at different wind speeds on the sea surface has been obtained. It can be seen that the simulation results are reasonable and effective.

3. EM Scattering of Sea Surface

3.1. EM Scattering of Nonbreaking Waves from Sea Surface. The refined facet scattering field model (RFSFM) proposed in this paper is used to calculate the scattering coefficient of nonbreaking waves on the sea surface. In the model, the scattering region of 2D sea surface is divided into two parts: specular region and nonspecular region. The facet-based asymptotical model (FBAM) [25] and Kirchhoff approximation method (KA) are used to calculate the scattering of facets located in the nonspecular region and specular region. Therefore, the scattering field of a facet can be expressed as follows:

$$E_{\mathrm{pq}}\left(\hat{k}_i, \hat{k}_s\right) = \begin{cases} E_{\mathrm{pq}}^{\mathrm{KA}}\left(\hat{k}_i, \hat{k}_s\right), & \text{specular region,} \\ E_{\mathrm{pq}}^{\mathrm{facet}}\left(\hat{k}_i, \hat{k}_s\right), & \text{nonspecular region,} \end{cases} \tag{2}$$

where the indexes of p and q denote the polarization of incident and scattering waves in the global coordinate system, respectively. The expression of $E_{\mathrm{pq}}^{\mathrm{KA}}$ is shown as follows:

$$E_{\mathrm{pq}}^{\mathrm{KA}}\left(\hat{k}_i, \hat{k}_s\right) = \frac{ik\,\exp(ikR)}{4\pi R}\hat{k}_s \times \int \left[(\hat{n} \times E) - \eta \hat{k}_s \times (\hat{n} \times H)\right] \cdot \exp\left[-ik\left(\hat{k}_s - \hat{k}_i\right) \cdot r'\right] \mathrm{d}S' = \frac{ik\,\exp(ikR)}{4\pi R} E_0 \cdot S_{\mathrm{pq}} \cdot I_{\mathrm{KA}}, \tag{3}$$

where $\hat{k}_i$ and $\hat{k}_s$ are, respectively, the unit vectors along the incidence and scattering direction; k is the wave number of electromagnetic waves; η is the impedance of the free space; $\hat{n}$ is the normal vector; R is the distance between the centre of facet and the observation point; E and H are the total electric field and magnetic field on the boundary surface; and E_0 is the amplitude of incident wave. The polarization factor S_{pq} and integral term I_{KA} can be expressed as

$$\begin{aligned} S_{\mathrm{pq}} = {} & -\hat{h}_i'\left(\hat{n} \cdot \hat{k}_i\right)\left(\hat{p} \cdot \hat{h}_i'\right)(1 - R_h) + \left(\hat{n} \times \hat{h}_i'\right)\left(\hat{p} \cdot \hat{v}'_i\right)(1 + R_v) \\ & + \left(\hat{k}_s \times \left(\hat{n} \times \hat{h}_i'\right)\right)\left(\hat{p} \cdot \hat{h}_i'\right)(1 + R_h) \\ & + \left(\hat{k}_s \times \hat{h}_i'\right)\left(\hat{p} \cdot \hat{v}'_i\right)\left(\hat{n} \cdot \hat{k}_i\right)(1 - R_v), \\ I_{\mathrm{KA}} = {} & \int_S \exp\left[-ik\left(\hat{k}_s - \hat{k}_i\right) \cdot r'\right] dS' = \frac{\Delta S}{n_z} e^{-iq \cdot r_0} \sin c\left(\frac{\Delta x}{2} q \cdot \hat{x}'\right) \\ & \cdot \sin c\left(\frac{\Delta y}{2} q \cdot \hat{y}'\right), \end{aligned} \tag{4}$$

where $\hat{h}'_i = \hat{k}_i \times \hat{n} / |\hat{k}_i \times \hat{n}|$ and $\hat{v}_i' = \hat{h}_i' \times \hat{k}_i$ are the polarization of incident wave in the local coordinate system. R_v and R_h are the Fresnel reflection coefficients. $\Delta S = \Delta x \Delta y$ is the area of facet on sea surface, wherein Δx and Δy are the intervals along x and y direction. r_0 is the facet's centre. n_z is the z component of the local normal vector $\hat{n}$. $q = k(\hat{k}_s - \hat{k}_i)$ is the scattering vector.

The expression of $E_{\mathrm{pq}}^{\mathrm{facet}}$ is shown as follows:

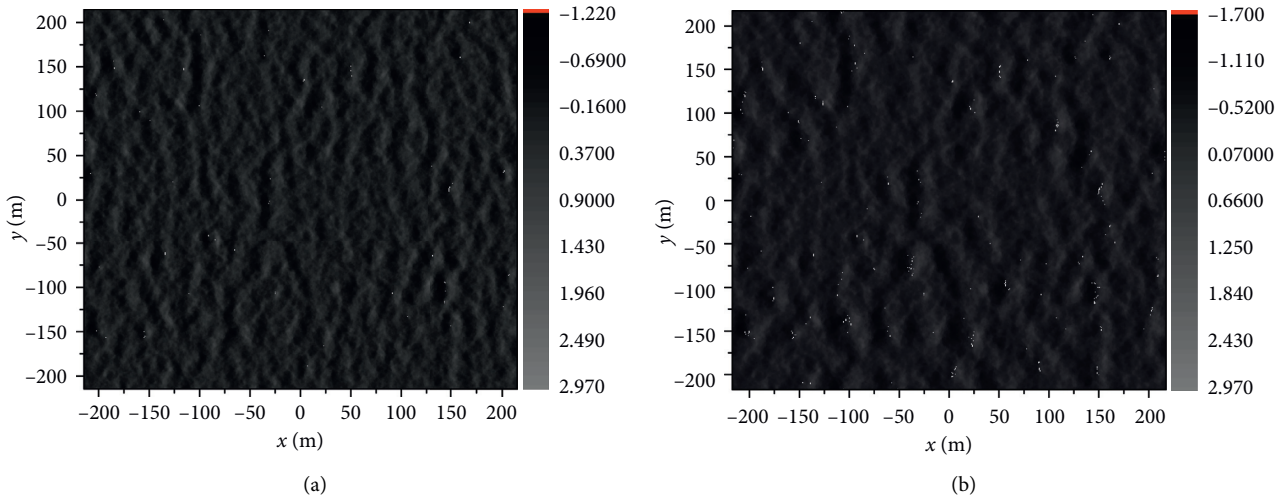

Figure 1: Distribution of breaking points on sea surface: (a) wind speed is 10 m/s; (b) wind speed is 15 m/s.

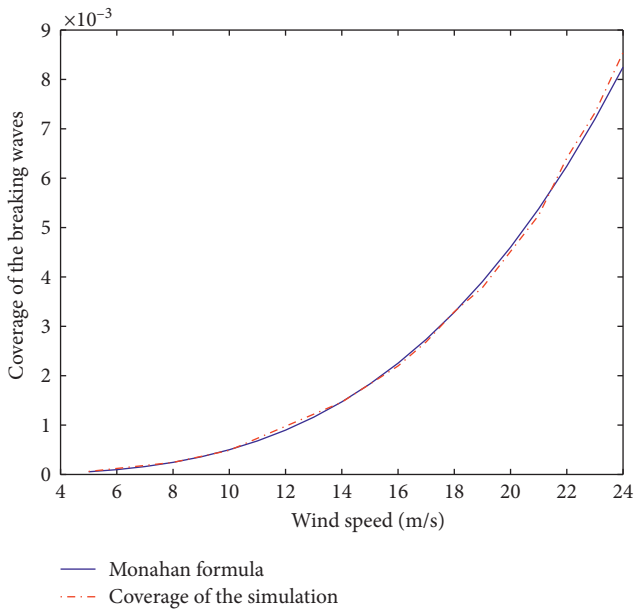

Figure 2: Comparison between the simulated coverage of the breaking waves and the measured model at different wind speeds.

$$E_{\mathrm{pq}}^{\mathrm{facet}}\left(\hat{k}_i, \hat{k}_s\right) = \frac{k^2(1-\varepsilon)}{2iR} e^{ikR} \cdot F_{\mathrm{pq}} \cdot I(\cdot), \tag{5}$$

where ε is the relative dielectric constant of sea water; F_{pq} is the polarization factor; and $I(\cdot)$ is an integral of the surface profile within a facet. The detailed expressions of F_{pq} and $I(\cdot)$ can be found in [25], which are omitted here due to space limitations.

Then, the total field from a whole sea surface could be obtained by the summation of the scattering fields from all the facets:

$$E_{\mathrm{pq}}^{\mathrm{sea}}\left(\hat{k}_i, \hat{k}_s\right) = \sum_{m=1}^{M} \sum_{n=1}^{N} E_{\mathrm{pq}}\left(\hat{k}_i, \hat{k}_s\right), \tag{6}$$

where M and N are the number of discrete points on the 2D sea surface, and the scattering model described in equation (2) is called the refined facet scattering field model (RFSFM). Therefore, the radar scattering coefficient σ_{n-wb} of sea surface without considering breaking waves can be obtained by

$$\sigma_{n-\mathrm{wb}} = \lim_{R \longrightarrow \infty} \frac{4\pi R^2}{A} \left[E_{\mathrm{pq}}^{\mathrm{sea}}\left(\hat{k}_i, \hat{k}_s\right) E_{\mathrm{pq}}^{\mathrm{sea}}\left(\hat{k}_i, \hat{k}_s\right)^* \right]. \tag{7}$$

3.2. EM Scattering of Breaking Waves from Sea Surface. Wave breaking is a complex and random process. In order to calculate the scattering coefficient of the breaking wave on the sea surface, in this paper, the model proposed by Kudryavtsev et al. [26] in 2003 is used to improve RFSFM, and then the influence of breaking waves on SAR imaging is studied. The scattering coefficient of breaking waves σ_{bw} can be expressed as

$$\sigma_{\mathrm{bw}} = \left(\frac{\sec^4 \overline{\theta}}{s_{\mathrm{wb}}^2} \right) \exp\left(-\frac{\tan^2 \overline{\theta}}{s_{\mathrm{wb}}^2} \right) + \frac{\varepsilon_{\mathrm{wb}}}{s_{\mathrm{wb}}^2}, \tag{8}$$

where $\overline{\theta}$ is the local incident angle of the facets; s_{wb}^2 is the mean-square slope of roughness enhancement at breaking waves; and $\varepsilon_{\mathrm{wb}}$ is the ratio of the thickness to the length of the breaking unit.

According to the EM scattering model of nonbreaking waves and breaking waves on the sea surface, the scattering coefficient of whole sea surface σ_{sea} can be obtained by

$$\sigma_{\mathrm{sea}} = \sigma_{n-\mathrm{bw}}(1-q) + \sigma_{\mathrm{bw}} q, \tag{9}$$

where q is the coverage rate of breaking waves.

Figure 3 shows the backscattering coefficients of sea surface with and without breaking waves. Figure 3(a) is with the wind speed of 7 m/s and Figure 3(b) is with 13 m/s. The incident frequency is 13.9 GHz. It can be seen from Figure 3 that the scattering coefficient at HH polarization is much smaller than the measured data [27] without

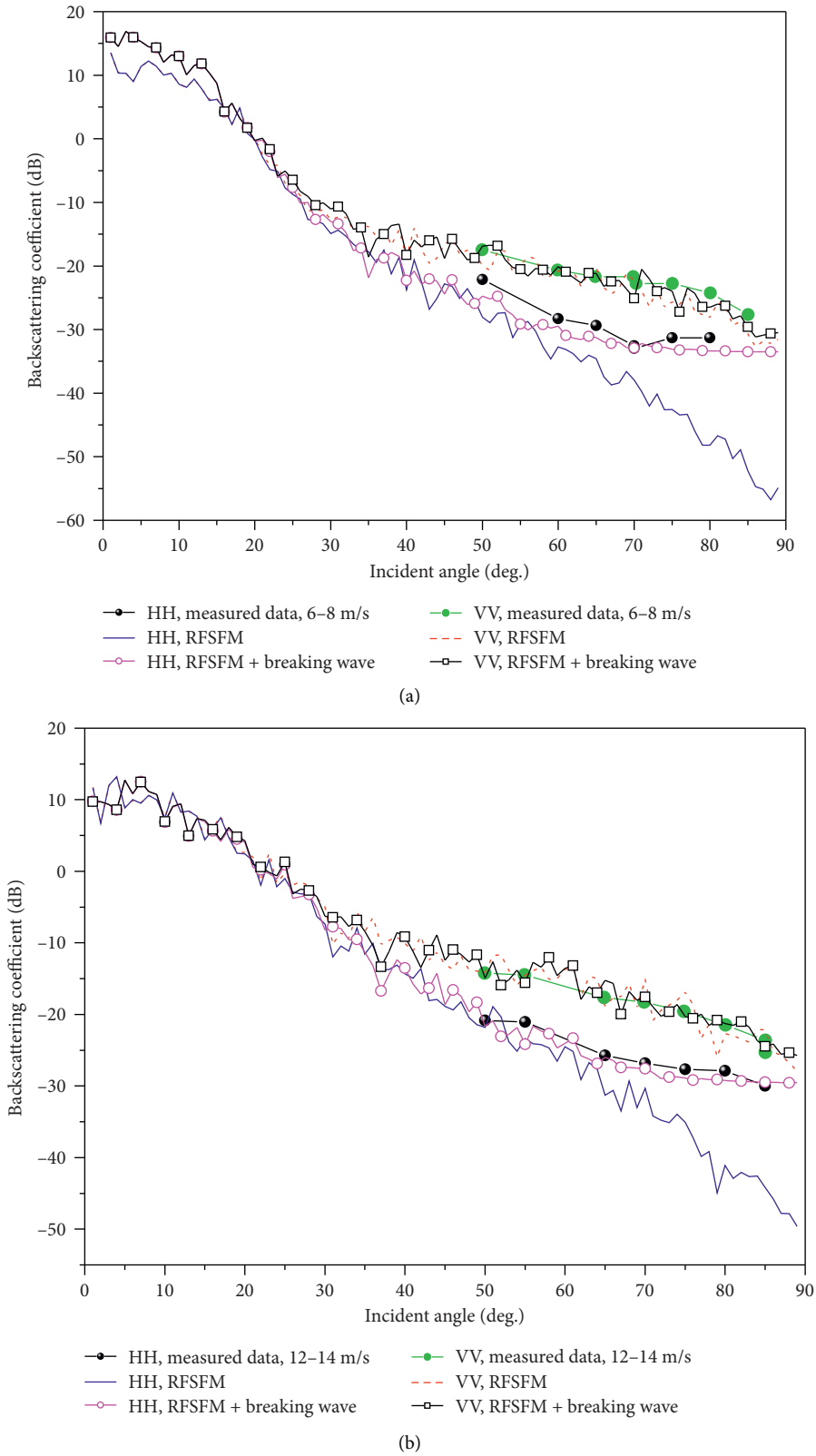

Figure 3: Comparisons of backscattering coefficient between the simulations and measured data: (a) wind speed is 7 m/s; (b) wind speed is 13 m/s.

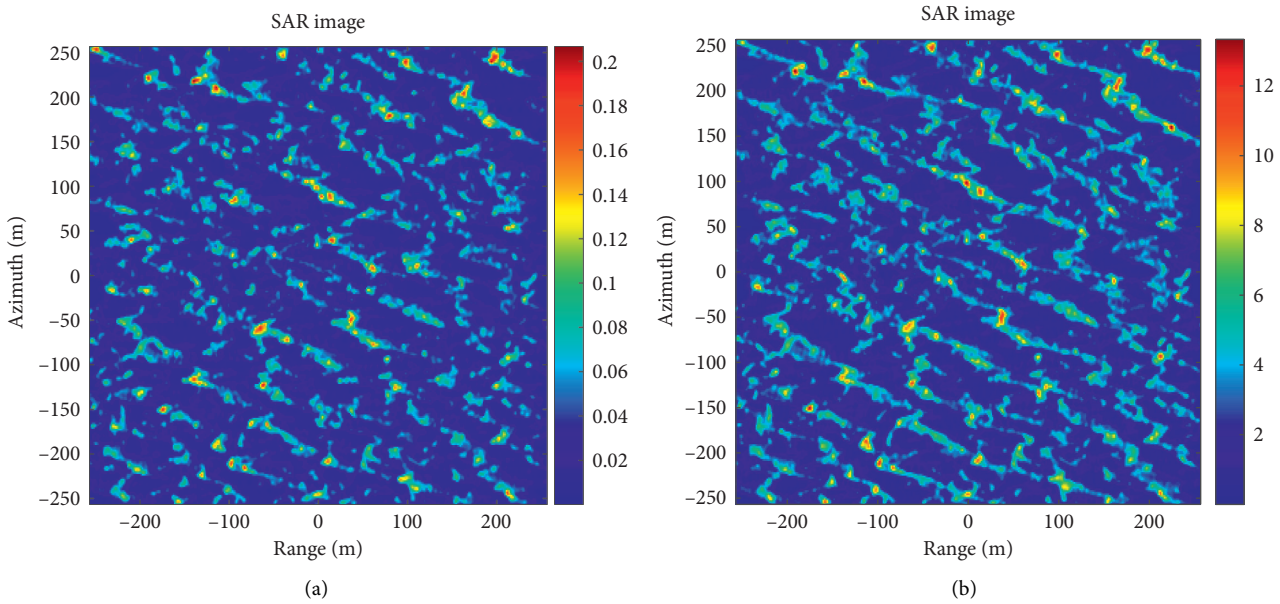

(a) (b)

Figure 4: The monostatic SAR image of sea surface without considering breaking waves: (a) HH polarization; (b) VV polarization.

considering the breaking waves. Taking the breaking waves into consideration, the scattering coefficient of HH polarization at large incident angle is greatly improved, which is more consistent with the measured data. As for VV polarization, the scattering contribution of breaking waves is relatively small.

3.3. SAR Image Simulation and Analysis at High Sea State. On the basis of the above model, the influence of breaking waves on mono/bistatic SAR imaging of sea surface is analyzed in this section under the conditions of different polarizations and different incidence angles. In general, SAR echo is related to the scattering coefficient of sea surface, which changes with time in the process of radar operation. Therefore, the random and time-varying characteristics of the sea surface make the simulation of SAR image have a certain complexity. For this reason, many scholars have done a lot of research work and put forward some approximate theories, and the commonly used model is the velocity bunching (VB) model proposed by Alpers [9]. In this paper, the velocity bunching (VB) model is used to simulate SAR image of sea surface with breaking waves. And, the intensity of SAR image at each position can be expressed as

$$
\begin{aligned}
I(x,y) &= B\int_{-L_x/2}^{L_x/2}\int_{-L_y/2}^{L_y/2} dx'dy'\sigma(x',y')\cdot\frac{\rho_{\mathrm{aN}}}{\rho'_{\mathrm{aN}}(x',y')}\cdot f_r(x-x') \\
&\quad\cdot\exp\left\{-\frac{\pi^2}{\rho'_{\mathrm{aN}}(x',y')^2}\left[y-y'-\frac{R\cdot u_r(x',y')}{V}\right]^2\right\}, \\
\sigma(x',y') &= \sigma_{\mathrm{sea}}\left[1+T_{\mathrm{vb}}(x',y')\right], \\
\rho'_{\mathrm{aN}}(x',y') &= \rho_{\mathrm{aN}}\left\{1+\frac{1}{N_l^2}\left[\left(\frac{\pi T^2}{\lambda}a_r(x',y')\right)^2+\left(\frac{T}{\tau_s}\right)^2\right]\right\}^{1/2}, \\
\rho_{\mathrm{aN}} &= N_l\cdot\frac{\lambda R}{2\mathrm{VT}},
\end{aligned}
\tag{10}
$$

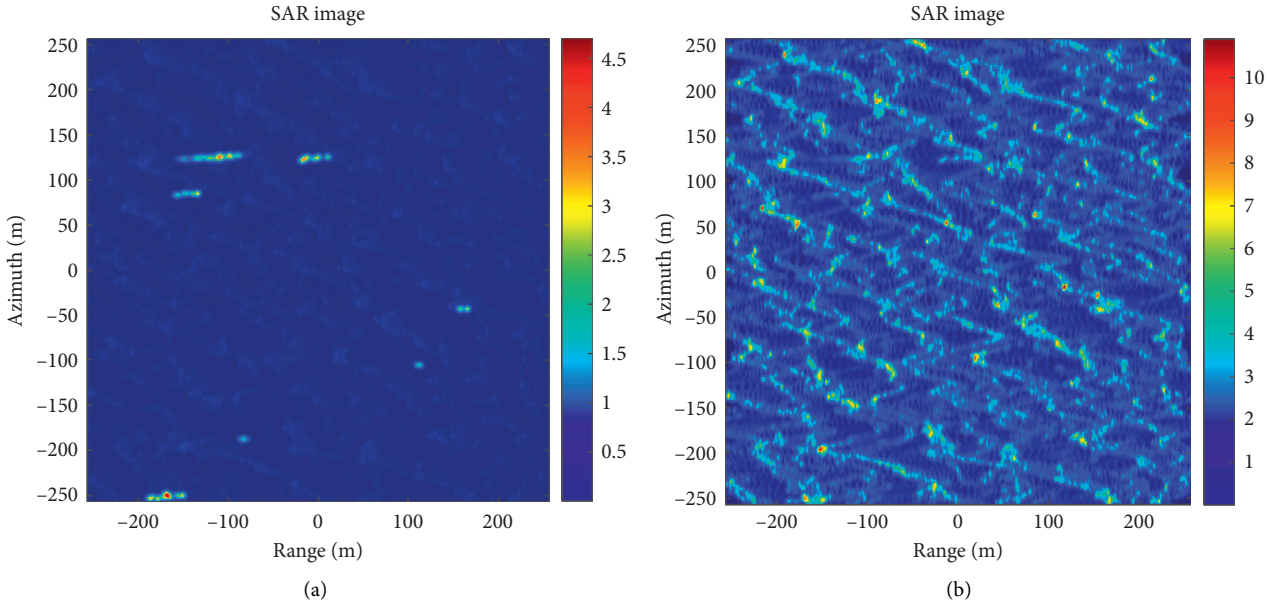

Figure 5: The monostatic SAR image of sea surface with considering breaking waves: (a) HH polarization; (b) VV polarization.

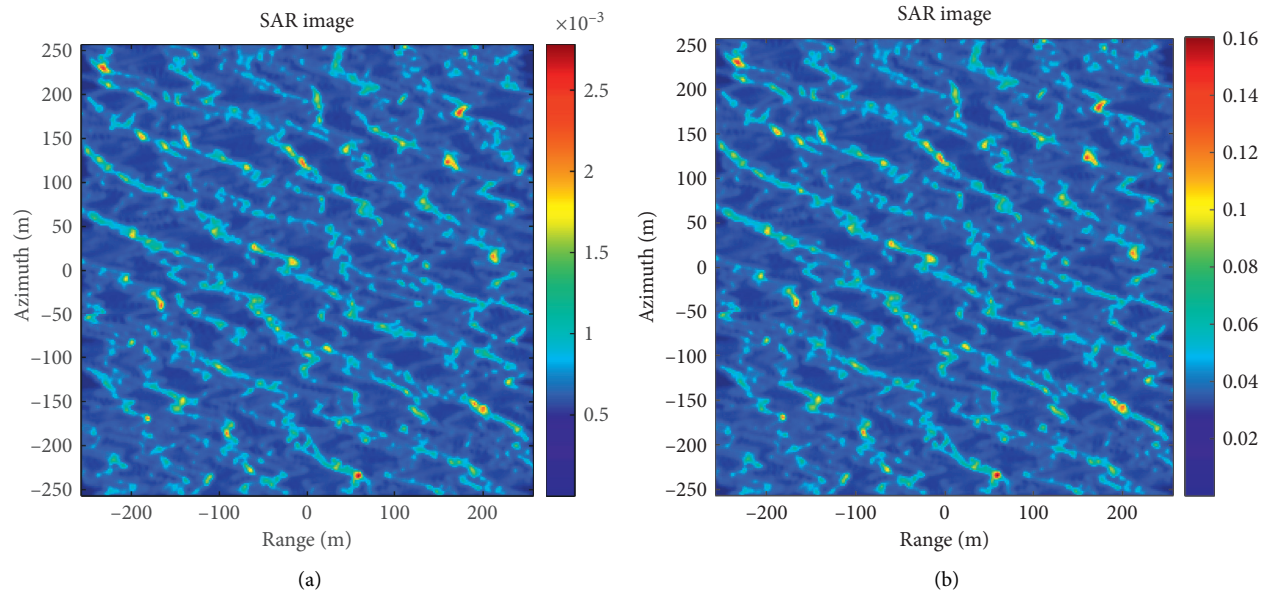

Figure 6: The bistatic SAR image of sea surface without considering breaking waves: (a) HH polarization; (b) VV polarization.

where $\sigma(x', y')$ represents the RCS after considering tilt modulation and velocity bunching modulation; T_{vb} is the velocity bunching modulation function; $f_r(\cdot)$ is the range resolution function; V is the speed of the radar platform; B is the gain of the radar antenna, and because its value does not affect the relative intensity of SAR image, the influence of B is ignored in this paper; u_r is the track speed along the observation direction; $\rho'_{\mathrm{aN}}(x', y')$ is the actual resolution after considering the target acceleration and limited coherent time; ρ_{aN} is the theoretical azimuthal resolution of a stationary target; N_l is the radar sight; λ is the radar wavelength; T is the integration time; τ_s is the scene coherence time; and a_r is the orbital acceleration along the observed direction.

If there are no special instructions, the 2D sea surface is generated using the nonlinear Creamer sea surface model, the sea surface area is $500m \times 500m$, and the relative dielectric constant of the sea water is calculated by the Klein model at 20°C and 35% salinity.

Figures 4 and 5, respectively, give the monostatic SAR image of sea surface at HH polarization and VV polarization without and with considering breaking waves. The incident frequency is 10 GHZ, the incident angle is 70°, the wind speed is 10 m/s, the total cumulative time is 0.25 s, and

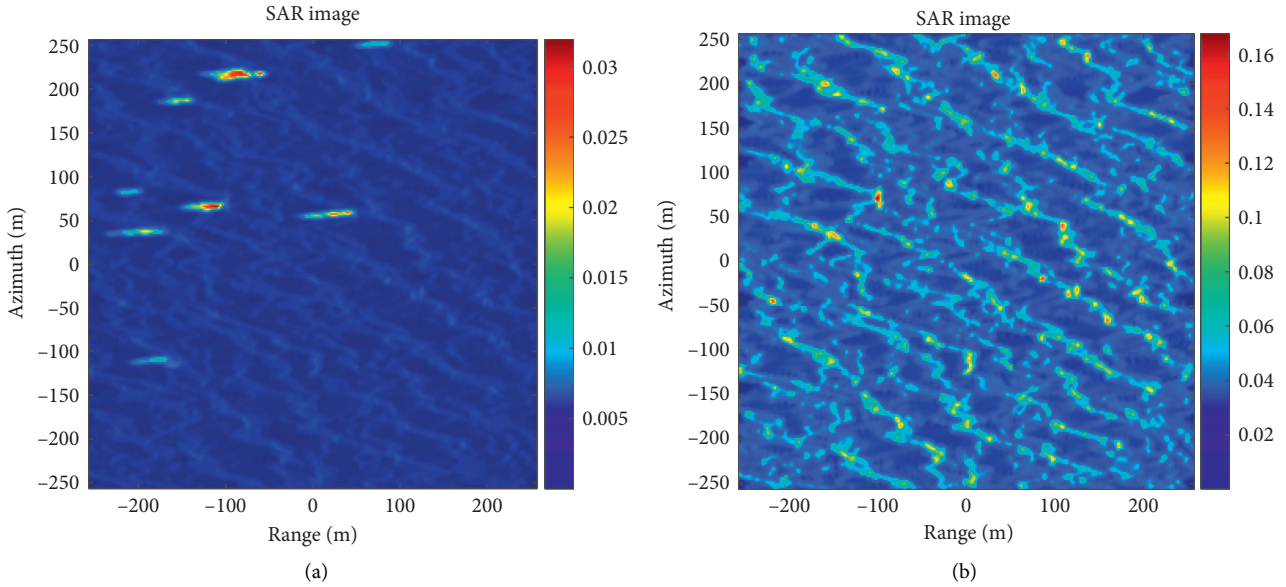

Figure 7: The bistatic SAR image of sea surface with considering breaking waves: (a) HH polarization; (b) VV polarization.

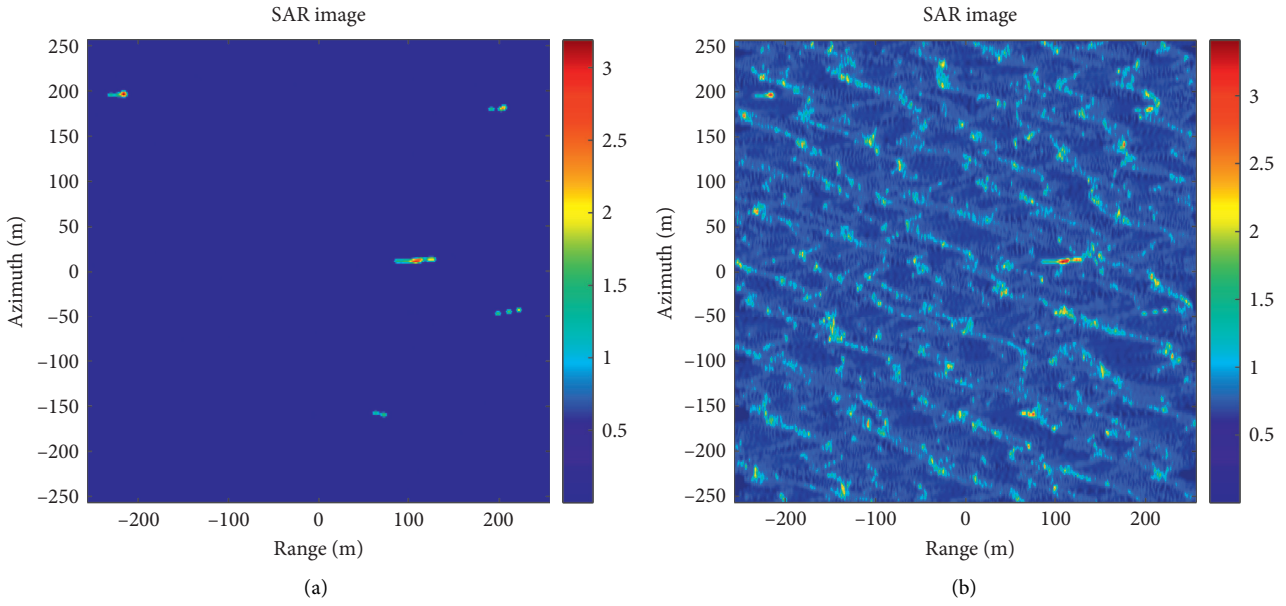

Figure 8: The monostatic SAR image of sea surface with considering breaking waves at large incident angle: (a) HH polarization; (b) VV polarization.

$R/V = 60$. As shown in Figures 4 and 5, one can see that the intensity of SAR image of sea surface with considering breaking waves at HH polarization is greatly enhanced. And SAR is more sensitive to the breaking waves at HH polarization. However, in the case of VV polarization, the variation of image intensity of monostatic SAR is not obvious, which is because that the influence of breaking waves on the scattering of sea surface at VV polarization is much smaller than that at HH polarization. In addition, the position distribution of breaking waves in SAR image is not the same as its geometric position, which is caused by the motion of breaking waves. Moreover, different breaking waves have different motion states, so their position changes are also different.

Figures 6 and 7, respectively, give the bistatic SAR image of sea surface at HH polarization and VV polarization without and with considering breaking waves. The incident frequency is 10 GHZ, the incident angle is 70°, the scattering angle is 60°, the wind speed is 10 m/s, the total cumulative time is 0.25 s, $(R/V)_T = 60$, and $(R/V)_R = 40$. It is worth noting that the bistatic SAR images of sea surface in Figures 6 and 7 have the same phenomenon with the

monostatic SAR images in Figures 4 and 5. Namely, when the breaking waves are considered, the intensity of bistatic SAR images at HH polarization is significantly greater. However, the change of image intensity is not obvious at VV polarization.

Figure 8 gives the monostatic SAR image of sea surface with considering breaking waves at large incident angle. The incident angle is 80°, and the wind speed is 10 m/s. From Figures 8(a) and 8(b), it can be found that with the increase in incident angle, the image intensity ratio of HH to VV polarization nearly reaches 1. As the incident angle continues to increase, the ratio will exceed 1. The maximum intensity of HH polarization is greater than that of VV polarization, which shows the phenomenon of high polarization ratio and sea peak; these similar phenomena are also shown in many real SAR images. Therefore, the model in this paper can be used to analyze the scattering of sea surface environment under high sea state.

4. Conclusion

In this paper, the improved scattering model of sea surface under high sea state was developed, which is the foundation for the investigation of the mono/bistatic SAR imaging of sea surface. With the help of RFSFM as well as the improved breaking wave model, the coverage of breaking waves on sea surface under different wind speeds is analyzed and the influence of breaking waves on the mono/bistatic SAR imaging of sea surface at HH polarization and VV polarization is analyzed in detail. The simulation results show that with the increase in wind speed, the coverage of breaking waves increases obviously, which is consistent with the situation of real sea surface. The mono/bistatic SAR is more sensitive to the breaking waves at HH polarization, and the intensity is greatly enhanced. In addition, the intensity ratio of HH to VV polarization is greater than or equal to 1 when the incident angle increases. However, at VV polarization, the graphic intensity of mono/bistatic SAR of sea surface did not increase greatly. Therefore, the improved model in this paper can modify the scattering of sea surface under high sea state and has certain application value.

Data Availability

The simulation data plotted in figures used to support the findings of this study are included within the article.

Conflicts of Interest

The authors declare that there are no conflicts of interest regarding the publication of this paper.

Acknowledgments

This work was supported in part by the National Natural Science Foundation of China (Grant nos. 61801416 and 62061048) and in part by the Scientific Research Foundation of Yan'an University (Grant no. YDBK2016-16).

References

[1] F. Luo, D. Zhang, and B. Zhang, "The fractal properties of sea clutter and their applications in maritime target detection," *IEEE Geoscience and Remote Sensing Letters*, vol. 10, no. 6, pp. 1295–1299, 2013.

[2] M. P. Clarizia, C. Gommenginger, M. Di Bisceglie, C. Galdi, and M. A. Srokosz, "Simulation of L-band bistatic returns from the ocean surface: a facet approach with application to ocean gnss reflectometry," *IEEE Transactions on Geoscience and Remote Sensing*, vol. 50, no. 3, pp. 960–971, 2012.

[3] P. A. Hwang, W. Perrie, and B. Biao Zhang, "Cross-polarization radar backscattering from the ocean surface and its dependence on wind velocity," *IEEE Geoscience and Remote Sensing Letters*, vol. 11, no. 12, pp. 2188–2192, 2014.

[4] J. Li, M. Zhang, P. Wei, and W. Jiang, "An improvement on SSA method for EM scattering from electrically large rough sea surface," *IEEE Geoscience and Remote Sensing Letters*, vol. 13, no. 8, pp. 1144–1148, 2016.

[5] B. Liu and Y. He, "SAR raw data simulation for ocean scenes using inverse omega-K algorithm," *IEEE Transactions on Geoscience and Remote Sensing*, vol. 54, no. 10, pp. 6151–6169, 2016.

[6] D. Schuler, J. S. Lee, D. Kasilingam, and E. Pottier, "Measurement of ocean surface slopes and wave spectra using polarimetric SAR image data," *Remote Sensing of Environment*, vol. 91, no. 2, pp. 198–211, 2004.

[7] A. Arnold-Bos, A. Khenchaf, and A. Martin, "Bistatic radar imaging of the marine environment-Part I: theoretical background," *IEEE Transactions on Geoscience and Remote Sensing*, vol. 45, no. 11, pp. 3372–3383, 2007.

[8] Y. Wang and Y. Zhang, "Investigation on Doppler shift and bandwidth of backscattered echoes from a composite sea surface," *IEEE Transactions on Geoscience and Remote Sensing*, vol. 49, no. 3, pp. 1071–1081, 2011.

[9] W. R. Alpers, D. B. Ross, and C. L. Rufenach, "On the detectability of ocean surface waves by real and synthetic aperture radar," *Journal of Geophysical Research*, vol. 86, no. C7, pp. 6481–6498, 1981.

[10] D. R. Lyzenga and R. A. Shuchman, "Analysis of scatterer motion effects in Marsen X band SAR imagery," *Journal of Geophysical Research: Oceans*, vol. 88, no. C14, pp. 9769–9775, 1983.

[11] R. O. Harger, "The SAR image of short gravity waves on a long gravity wave," in *Wave Dynamics and Radio Probing of the Ocean Surface*, O. M. Phillips and K. Hasselmann, Eds., Springer, Boston, MA, USA, pp. 371–392, 1986.

[12] F. Nunziata, A. Gambardella, and M. Migliaccio, "An educational SAR sea surface waves simulator," *International Journal of Remote Sensing*, vol. 29, no. 11, pp. 3051–3066, 2008.

[13] M. Migliaccio, L. Huang, and A. Buono, "SAR speckle dependence on ocean surface wind field," *IEEE Transactions on Geoscience and Remote Sensing*, vol. 57, no. 8, pp. 5447–5455, 2019.

[14] I. Rizaev, O. Karakuş, S. J. Hogan, and A. Achim, "Modeling and SAR imaging of the sea surface: a review of the state-of-the-art with simulations," 2021, https://arxiv.org/abs/2102.05199.

[15] G. J. Diao, X. J. Xu, H. Ni, and J. J. Lu, "Synthetic aperture radar signal simulation of ships on sea surface," *Journal of System Simulation*, vol. 27, no. 9, pp. 1989–1997, 2015, Chinese.

[16] Y.-Q. Jin and Z. Li, "Bistatic scattering and transmitting through a fractal rough dielectric surface using the forward

and backward method with spectrum acceleration algorithm (Fbm/Saa)," *Journal of Electromagnetic Waves and Applications*, vol. 16, no. 4, pp. 551–572, 2012.

[17] M. Zhang, Y.-W. Zhao, Y. Zhao, and H. Chen, "A bistatic synthetic aperture radar imagery simulation of maritime scene using the extended nonlinear chirp scaling algorithm," *IEEE Transactions on Aerospace and Electronic Systems*, vol. 49, no. 3, pp. 2046–2054, 2013.

[18] Y. Zhao, M. Zhang, Y.-W. Zhao, and X.-P. Geng, "A bistatic SAR image intensity model for the composite ship-ocean scene," *IEEE Transactions on Geoscience and Remote Sensing*, vol. 53, no. 8, pp. 4250–4258, 2015.

[19] J. C. West, "Correlation of Bragg scattering from the sea surface at different polarizations," *Waves in Random and Complex Media*, vol. 15, no. 3, pp. 395–403, 2007.

[20] A. G. Voronovich and V. U. Zavorotny, "Theoretical model for scattering of radar signals in Ku- and C-bands from a rough sea surface with breaking waves," *Waves in Random Media*, vol. 11, no. 3, pp. 247–269, 2001.

[21] P. A. Hwang, B. Zhang, J. V. Toporkov, and W. Perrie, "Comparison of composite Bragg theory and quad-polarization radar backscatter from RADARSAT-2: with applications to wave breaking and high wind retrieval," *Journal of Geophysical Research Oceans*, vol. 115, no. C8, pp. 246–255, 2010.

[22] J. Li, M. Zhang, W. Fan, and D. Nie, "Facet-based investigation on microwave backscattering from sea surface with breaking waves: sea spikes and SAR imaging," *IEEE Transactions on Geoscience and Remote Sensing*, vol. 55, no. 4, pp. 2313–2325, 2017.

[23] M. S. Longuet-Higgins and N. D. Smith, "Measurement of breaking waves by a surface jump meter," *Journal of Geophysical Research Oceans*, vol. 88, no. C14, pp. 9823–9831, 1983.

[24] E. C. Monahan, "Whitecaps and foam," *Encyclopedia of Ocean Sciences*, pp. 331–336, 2001.

[25] Y. Zhao, X.-F. Yuan, M. Zhang, and H. Chen, "Radar scattering from the composite ship-ocean scene: facet-based asymptotical model and specular reflection weighted model," *IEEE Transactions on Antennas and Propagation*, vol. 62, no. 9, pp. 4810–4815, 2014.

[26] V. Kudryavtsev, D. Hauser, G. Caudal, and B. Chapron, "A semiempirical model of the normalized radar cross-section of the sea surface 1. Background model," *Journal of Geophysical Research Oceans*, vol. 108, no. C3, pp. FET 2-1–FET 2-24, 2003.

[27] W. J. Plant, "Microwave sea return at moderate to high incidence angles," *Waves in Random and Complex Media*, vol. 13, no. 4, pp. 339–354, 2006.